Electrochromic Thin Films of the V-Cr Prussian Blue Analogue Molecular Magnet

Electrochromic Thin Films of the V-Cr Prussian Blue Analogue Molecular Magnet

Luke Hedley, Neil Robertson, J. Olof Johansson*

EaStCHEM, School of Chemistry, University of Edinburgh, David Brewster Road, EH9 3FJ, UK

**Corresponding author. Email address: olof.johansson@ed.ac.uk*

Abstract: This paper describes spectroelectrochemical measurements of thin films of the $V^{II/III}$-Cr^{III} Prussian blue analogue (V-Cr PBA). We show that we can electrically control the optical properties of this room-temperature molecule-based magnet and reversibly switch the colour of the films from blue to black upon reduction. The cyclic voltammogram of the films showed a weak wave at −0.85 V and a stronger wave at −1.22 V. The spectroelectrochemical measurement in KCl indicate that the wave at −0.85 V is related to the reduction of V(III) to V(II) because of a shift in the absorption band associated with the metal-to-metal charge-transfer band. The wave at −1.22 V occurred simultaneously with the growth of a new absorption feature at 465 nm and is attributed to the reduction of $[Cr^{III}(CN)_6]^{3-}$ sites to $[Cr^{II}(CN)_6]^{4-}$. We have assigned the change to the optical spectrum occurring at 465 nm after electrochemical reduction to a red-shift of a metal-to-ligand charge-transfer (MLCT) transition from Cr^{2+} to empty π* ligand orbitals. The electrochromic coloration efficiency associated with switching from blue to black colour was found to be $\eta = -25.2 \pm 0.2$ cm^2 C^{-1} with a switching time of 6.6 s at −1.3 V. These findings

demonstrate the possibility to electrically control the optical properties of a room-temperature molecular magnet.

Keywords: Electrochromism; spectroelectrochemistry; Prussian blue analogues; molecular magnetism

1. Introduction

The colour of electrochromic materials can be switched by applying a small electrical voltage [1,2]. These materials show large potential to be used in electrochromic windows and mirrors, sensors, or light modulators. For light modulators, additional magnetic ordering of the materials would also allow for modulating the light polarisation via the Faraday effect [3]. Here we have explored a family of molecular materials whose magnetic properties can be switched electrochemically and at the same time show electrochromic effects. In order to develop future multi-functional devices combining magnetic and electrochromic properties, there is an urgent need to gain a deep understanding of the spectroelectrochemical properties of these materials. An additional advantage of molecular materials is that they can be made transparent and be deposited on glass substrates. More generally, solution-processed electrochromic materials are gaining in popularity since they require less energy in the manufacturing process [4].

Some of the most studied molecule-based magnets are Prussian blue and its analogues, which comprise transition metal ions linked by cyanide ligands in a rock-salt structure [5]. The general formula is $C_cA_a[B(CN)_6]_b \cdot nH_2O$ (C=alkali cation, A,B =

transition metal ions). Thin films of these magnetic materials have previously been electrochemically deposited on conductive glass substrates for a range of analogues [3,6–11]. The original Fe-Fe Prussian blue has been studied extensively for electrochromic applications [1,2]. Other PBAs, mainly containing hexacyanoferrate, have also been explored and an extensive summary is presented in Ref. [12]. Interestingly, some PBAs can be reversibly switched between a ferrimagnetic and paramagnetic state electrochemically [13–15]. For combining optical and magnetic functionality, the V-Cr PBA is promising because it is ferrimagnetic at room temperature [16] and has a clear blue colour. Verdaguer *et al*. have observed electrochromic behaviour of this material and showed that it is possible to change the colour from blue to colourless upon oxidation [17,18]. The aim of the work presented here was to expand the range of electrochromic switching capabilities of the V-Cr PBA and to understand the mechanisms involved causing the change to the optical spectrum as a function of applied potential. We have therefore studied the spectroelectrochemistry of the films at a more reducing potential than Verdaguer *et al*. and found that we could reversibly switch the colour from blue to black. We have assigned the absorption giving rise to the black colour and determined the colouration efficiency and the switching time for the blue-to-black electrochromic response.

The oxidation state of the vanadium ions in the V-Cr PBA can vary depending on the synthetic conditions and often both V(II) and V(III) are found. Typically, the materials are to a large degree amorphous and characterisation is challenging due to the high air sensitivity. Nevertheless, oxidation states of the vanadium ions have been determined using X-ray absorption spectroscopy (XAS) [19], energy-dispersive x-ray spectroscopy (EDS) and x-ray photoelectron spectroscopy (XPS) [20], and elemental

analysis [8] (based on charge-balance arguments). The visible spectrum of the V-Cr PBA is dominated by strong metal-to-metal charge-transfer (MMCT) bands, where an electron is optically transferred from a Cr ion to a V ion. More energy is required to transfer an electron from a Cr ion to a V(II) site than to a V(III) site. The spectral position of the MMCT therefore depends on the oxidation state of the vanadium ions. Garde *et al*. found that for V-Cr PBAs containing solely V(II), the main MMCT transition occurred at 540 nm, whereas in samples comprising only V(III), the absorption occurred at 650 nm [19]. For electrochemically produced films, Ohkoshi *et al*. [8] also noted that for certain conditions, they could produce predominantly V(II), which resulted in an absorption peak at 540 nm, in agreement with Garde *et al*. [19]. When Ohkoshi's films contained both V oxidation states, peaks at both 540 and 660 nm were observed. Another feature to note in the absorption spectrum of V-Cr PBA is a peak at 800 nm that has been assigned to a forbidden d-d transition localised on the $[Cr^{III}(CN)_6]^{3-}$ ions, which becomes partly allowed in the PBA network [19]. There are intense bands below 400 nm, which have been assigned to ligand-to-metal (LMCT) and metal-to-ligand (MLCT) charge-transfer transitions due to their energy and relatively strong oscillator strength [21,22].

The paper is organised as follows. In Section 2, the experimental approach is briefly explained and we discuss the synthetic methods and how to protect the air sensitive films. In Section 3.1, we present the cyclic voltammograms (CVs) of both the starting materials and the final films. The characterisation of these films is subsequently described in Section 3.2. We found that we can control the film thickness by varying the deposition time and interestingly we found that in thinner film it is possible to distinguish the V oxidation states in the transmittance spectrum. The dependence of the transmittance spectrum as function of applied voltage was studied in a

spectroelectrochemical measurement and the results are presented in Section 3.3. We found that for lower voltages, we observe an increase in the MMCT associated with the Cr(III) to V(II) transition as a consequence of the reduction of V(III) to V(II). For more negative voltages, a MLCT absorption on the Cr ions is observed as a consequence of reducing $[Cr^{III}(CN)_6]^{3-}$ to $[Cr^{II}(CN)_6]^{4-}$. We have characterised the electrochromic performance of the films by investigating the colouration efficiency and switching time in Section 3.4. These results show a new electrochemical control of the optical properties of the magnetic V-Cr PBA.

2. Experimental

The films were electrochemically deposited on fluorine-doped tin oxide (FTO) coated glass substrates of 1 mm thickness. The substrates were sequentially cleaned in an ultrasonic bath in the following solvents: deionised water and detergent, isopropanol, methanol, and finally in deionised water, since water is used as solvent in the electrochemical cell. All electrochemical experiments were carried out using a Metrohm-Autolab μAUTOLABIII potentiostat with a saturated calomel reference electrode and a Pt counter electrode. Aqueous solutions of VCl_3 and $K_3[Cr(CN)_6]$ from Sigma-Aldrich were used without further purification at concentrations typically 10 mM and KCl (also from Sigma-Aldrich) was used as electrolyte at a concentration of 1.0 M. The V-Cr PBAs are air sensitive and so the electrochemistry was performed under N_2 flow. All solvents were thoroughly bubbled with N_2 and any O_2 in the reagent powders were removed using a Schlenk line. The films were made under potentiostatic conditions, typically at −1.15 V vs SCE. After the synthesis, the films were rinsed with N_2-bubbled H_2O and allowed to dry under N_2 flow. Once dried, they were either sealed with cyanoacrylate glue and a 0.18 mm thick glass microscope coverslip or immediately used for CV scans without sealing. The film area typically

ranged from 1.0 to 1.2 cm^2. Spectroelectrochemistry measurements were carried out in a standard 10 mm cuvette. A fibre-based halogen light source (Ocean Optics HL-2000-FHSA) and a fibre-coupled spectrometer (Ocean Optics HR2000+) were used. The films, together with reference and counter electrodes, were immersed in the cuvette. In order to fit all the electrodes, the saturated calomel reference electrode was replaced with a pseudo-reference electrode made from Pt wire. Any shift in potential of the pseudo-reference electrode was checked in a normal electrochemical cell with either the Pt electrode or the SCE electrode by carrying out a CV scan of a V-Cr PBA film. A shift smaller than 0.02 V was observed.
Electrochromic characterisation was carried out by setting the spectrometer to measure at a fixed wavelength at 465 nm and was synchronised with the potentiostat, which in turn was programmed to cycle the potential between 0 and −1.3 V at 15 s intervals.

The IR spectra were acquired using an attenuated total reflection IR spectrometer (Perkin Elmer Spectrum Two – UATR) by scraping off the films from the glass substrates with a razor blade. For the XPS measurements, the samples were freshly prepared and stored in N_2-bubbled water and were quickly transferred to the XPS where they were allowed to dry in the vacuum of the instrument. The sample was grounded by contacting the FTO-surface to ground using a metal support. The films were measured first without any surface treatment and subsequently after sputtering with Ar^+ ions for 30 min. The XPS instrument, VG Scientific with an Al Kα radiation source, was calibrated based on Cu $2p_{3/2}$ standard. Normally adventitious carbon would be used to further calibrate the spectrum for a specific sample. However, since there is probably a mixture of adventitious and cyanide carbon we did not further fine-tune the calibration. The C 1s peak positions before and after sputtering

were 284.7 and 284.4 eV, respectively. Because the C 1s peaks were reasonably close to that expected for carbon (either cyanide or adventitious), the calibration was sufficiently accurate to distinguish Sn, V, and Cr. A Shirley baseline was subtracted from the XPS spectra and Gaussian functions were used to fit the peak area and positions. The AFM measurements were carried out on a freshly made sample that was immediately transferred to the AFM (AFM Veeco Nanoman VS with Dimension 3100 controller). However, it was not possible to purge the AFM with N_2 and so all AFM measurements were carried out on oxidised films.

3 Results and discussion

3.1 Electrochemical synthesis

When making the films, we followed the approach of Ohkoshi *et* al., who used potentiostatic conditions at a relatively large negative potential (−1.16 V vs SCE) [8]. We found that this method leads to the best optical quality and the clearest blue colour of the V-Cr PBA films. Aqueous solutions of VCl_3 and $K_3[Cr(CN)_6]$ were made and added to the electrochemical cell along with the electrolyte. When applying a negative potential to the working electrode, V^{3+} ions are reduced at the electrode surface to produce V^{2+} ions. These ions subsequently react with $[Cr(CN)_6]^{3-}$ units in the solution to form the insoluble PBA film on the electrode surface. In order to understand the electrochemical synthesis, we first carried out the CV of the individual starting materials separately, *viz* VCl_3 and $K_3[Cr(CN)_6]$. The results are presented in Fig.1 (a) and (b). In the CV for $K_3[Cr(CN)_6]$, shown in Fig. 1 (a), the weak reduction peaks at −0.7 and −1.1 V were negligible compared to the currents recorded for VCl_3 and are attributed to impurities. As can be seen in Fig. 1 (a), the reduction of the V ions appears around −0.8 V. The reverse process corresponds to

the re-oxidation of V(II) ions. When scanning to more negative voltages (Fig. 1 (b)), which are used during the synthesis of the V-Cr PBA films, a more complicated CV is observed. We attribute the second reduction wave at −1.1 V to the nucleation of vanadium-containing deposit on the working electrode, which is an important step towards forming the insoluble PBA films on the substrate surface. The sharp re-oxidation peak at −0.5 V is then the stripping peak of the vanadium-containing deposit formed on the substrate, which is not observed when the potential is scanned only to −0.8 V. The oxidation of free V(II) ions can still be seen at the broad peak around 0 V. When the electrochemical synthesis is carried out in the presence of the two reagents together, the CV is different (Fig. 1 (c)). The stripping peak is significantly reduced in intensity, which is due to a kinetic effect where the V^{2+} ions react more readily with the $[Cr(CN)_6]^{3-}$ rather than to continue to plate vanadium-containing deposits onto the substrate surface. This is therefore consistent with the formation of V ions attached to the substrate in order to form the insoluble PBA film. Note that we do not normally cycle the voltage when making V-Cr PBA films for optical applications since we found that the best optical quality, as previously mentioned, is produced at potentiostatic conditions at as negative potential as possible (*ca*. −1.15 V). It should be noted however that Verdaguer *et al*. followed a different approach by using VO^{2+} as a starting material and subsequently grew the films by cycling the potential between −0.6 and 0.1 V vs. SCE [17]. In order to distinguish processes involved in the film formation during the CV scan in Fig. 1 (c) and the CV of the final film produced potentiostatically, the CV of the potentiostatically produced PBA film was repeated in KCl electrolyte from 1.0 to −1.3 V. The results of the potentiostatic deposition and subsequent cycling in KCl are presented in Fig. 2 (a) and (b). For the measurements presented here, the films were

made by applying a static potential at −1.15 V for 3 min. In the CV a wave at −0.85 V is observed and we attribute this to the reduction of V(III) present in the film. XPS measurements presented below indicate that V(III) is indeed present in the final film at a relatively high concentration. The reduction of V(III) sites is further supported by the spectroelectrochemical data presented in Section 3.3. The large wave at −1.22 V is attributed to the reduction of $[Cr^{III}(CN)_6]^{3-}$ to $[Cr^{II}(CN)_6]^{4-}$, with the corresponding re-oxidation taking place at −1.05 V. During the CV procedure, charge balance is maintained by the insertion and extraction of potassium counter ions (SI). The CV could be repeated several times. However, the peak current decreases slightly for each cycle due to film dissolution. This reduction process has not been discussed previously for the V-Cr PBA but it has been shown that $[Cr^{III}(CN)_6]^{3-}$ can be reduced at a similar potential in the Fe-Cr PBAs (−1.15 V vs. SCE) [23]. In Cr-Cr PBA, however, the reduction of $[Cr^{III}(CN)_6]^{3-}$ is thought to happen at a less negative potential (−0.85 V vs. Ag/AgCl) [9,11]. It is therefore possible that the first wave at −0.85 V is the reduction of $[Cr^{III}(CN)_6]^{3-}$. However, based on the spectral changes of the MMCT transition associated with this reduction wave, we attribute the first −0.85 V to the V(III) to V(II) reduction process, as is discussed below.

3.2 Film characterisation

The films were characterised with XPS, UV/VIS and IR spectroscopy. The XPS data are presented in Fig. 3 (a) for the full range of electron binding energies recorded. The expected elements such as C, N, O, Cr and V were observed, as well as the Sn peaks from the FTO layer. We did not observe any K or F peaks. The region around the expected vanadium peaks is shown in Fig. 3 (b). Here three peaks were used to fit the V $2p_{3/2}$ peaks in order to capture the relative intensities of the contributions

from V(II), V(III), and the oxidised V(IV). The spin-orbit split peaks corresponding to $2p_{1/2}$ appear to ca. 7.5 eV higher binding energies. Unfortunately, the resolution of the measurement was not good enough to distinguish between V(II) and V(III), however the V(IV) peak at 517.1 eV could be distinguished from the two other valences. Because of the air sensitivity of the materials, it is natural to assume that a thin oxide layer is formed on top of the films. In fact, the band maximum of the V peaks is shifted towards the binding energy of 517.1 eV associated with oxidised vanadium. The film was therefore sputtered with Ar^+ ions for 30 min. After sputtering, the V band maximum has clearly shifted towards the range 513.6 eV (marked with a dashed line in the figure) to *ca*. 515.8 eV, associated with V(II) and V(III). The peak from oxidised vanadium at 517.1 eV is much less pronounced than in the spectrum from the non-sputtered surface. Despite the poor resolution, it is clear that the sputtered spectrum contains much less oxidised material than the non-sputtered spectrum (from the untreated surface). Since the relative V oxidation states could not be resolved, the composition of the V-Cr PBA film was determined based on the total area of V and Cr peaks in the XPS spectra. The peak areas were compared after correcting for the atomic sensitivity factors and taking into account the accuracy of the technique. A Cr:V ratio of 0.8 was found for the sputtered sample. Based on these findings, and assuming that the film should be neutral, we can determine the composition of the films as $\mathrm{V}^{\mathrm{II}}_{0.5}\mathrm{V}^{\mathrm{III}}_{0.5}[\mathrm{Cr}^{\mathrm{III}}(\mathrm{CN})_6]_{0.8}$. The composition of the non-sputtered film was $\mathrm{V}^{\mathrm{II}}_{0.1}\mathrm{V}^{\mathrm{III}}_{0.9}[\mathrm{Cr}^{\mathrm{III}}(\mathrm{CN})_6]_{0.9}$. In order to maintain the charge balance, potassium ions can be found in the lattice depending on stoichiometry. The XPS does not show any potassium ions although small amounts could potentially be difficult to detect since this peak is masked by the much stronger C signal. Nevertheless, we rule out any significant concentration of K^+ ions in the sample and

so the charge balance is achieved by a slightly smaller amount of Cr to V and mixture of V oxidation states. The larger contribution of V(III) on the un-treated surface can be due to oxidised V(II). Furthermore, V(III), which is present in the solution, can react more readily with the already formed V-Cr PBA lattice. It is therefore likely that the majority of the V(III) sites are located at the surface of thicker films, as is indeed confirmed by the depth-dependent XPS measurements made possible with sputtering. The $2p_{3/2}$ Cr peak appears at 577.9 eV for the non-sputtered measurement and at 574.8 eV for the sputtered measurement (with a weak shoulder still observable at *ca*. 577 eV). The Cr $2p_{1/2}$ peak occurs at 584.9 eV for the sputtered measurement, giving a spin-orbit splitting of 10.1 eV. The Cr-peak binding energy is close in value to that reported by Hatlevik *et al*. (577.2 eV) [20] for non-sputtered films. However, in the spectrum for the sputtered surface we observe a binding energy closer to that expected for $[Cr^{III}(CN)_6]^{3-}$, which occurs at 576.2 eV [9]. Clearly the environment for the Cr ions at the surface is different from inside the bulk film.

Because the Cr:V ratio ranges from 0.8 to 0.95 (sputtered or non-sputtered, respectively), it indicates that there are few vacant sites in the lattice.

The presence of the V-Cr PBA network is confirmed by the IR spectrum shown in Fig. 3 (c). The Cr^{III}-C≡N-V^{II} peak has previously been reported to occur at around 2104 cm^{-1} and the Cr^{III}-C≡N-V^{III} peak at 2118 cm^{-1} [16]. The cyanide stretching peak in Fig. 3 (c) can be seen at 2113.5 (4) cm^{-1} (32 cm^{-1} FWHM), which is in agreement with previously reported values for the V-Cr PBA [16]. Given the width of the peak at 2113.5 cm^{-1}, we can conclude that the IR data support the presence of both vanadium oxidation states. The peak at 2175.6 (2) cm^{-1} (with 30 cm^{-1} FWHM) is due to the presence of vanadyl and is an indication that the films are oxidised when they

are exposed to air during the IR measurement. Powder X-ray diffraction patterns, obtained by scraping off the films from the substrate surface, were nearly featureless and so indicate that the films are mainly amorphous.

The film thickness was determined from the AFM measurements presented in Fig. 4 (a) and (b). The thickness could be controlled by the duration of the potentiostatic deposition process and four different deposition times were investigated (1 to 4 minutes). The AFM measurements were carried out with a freshly prepared sample which was transported from the synthesis lab to the AFM instrument in a sealed container. However, the samples oxidised during the measurement, as is apparent by the change in colour (the films become white/brown within 5 minutes in air). Ferlay *et al*. [24] have made structural measurements of the oxidised vanadyl analogue, and they observed a cubic structure with lattice parameter of ca. a = 10.490 (4) Å, similar to the non-oxidised V-Cr PBA sample. We therefore believe that the thickness measured on the oxidised sample is similar to the non-oxidised sample. For the thinnest film, a distribution of particles with a wide size distribution from *ca.* 25 to 90 nm was found (with an average size of 50 nm). However, for longer deposition times, a more continuous film was grown. The continuous films appear to crack when oxidised, which was observed for all films grown for longer than 1 minute. This is shown in Fig. 4 (b) for the film deposited for 2 minutes. From the size distribution of the particle size in Fig. 4 (a) (film deposited for 1 minute) and the depth of the cracks of the thicker films, we could estimate the film thickness as a function of deposition time, which is presented in Fig. 4 (c). In order to relate the optical density to the film thickness, the transmittance was recorded for each film before they were oxidised. The results are presented in Fig. 4 (d). It is interesting to notice that for the

thinnest film, the MMCT transitions to the two different vanadium oxidation states can clearly be seen as minima in the transmittance at 540 and 660 nm. However, for the thicker films, the two MMCT bands merge together. For the longest deposition time, the corresponding absorption reached an optical density of 4.0 (seen as zero transmittance on the scale in Fig. 4 (d)). In order to compensate for different ratios of V(II):V(III), which can depend on the film thickness as was discussed in the XPS section, the total transmittance over both MMCT peaks was integrated. According to the Beer-Lambert law, the transmittance scales exponentially with the optical path length and so the logarithm S of the integrated transmittance from 500 to 750 nm, should therefore produce a linear relationship with film thickness d according to

$$S = \ln\left(\int_{500\,\mathrm{nm}}^{750\,\mathrm{nm}} T(\lambda)\mathrm{d}\lambda\right) \propto d. \qquad (1)$$

We therefore plotted the natural logarithm of the integrated transmittance in Fig. 4. (e). A linear dependence is observed, in agreement with the AFM images of the oxidised films. We also plotted the total charge deposited for each film. In principle this should correlate with the total amount of material deposited. Based on an area of 1 cm^2 we would need *ca*. 10^{16} electrons to produce one sheet of the V-Cr PBA (assuming that each V ion is 10 Å apart). This estimation also assumes that all vanadium is present as V(II). Since the deposited films were grown with a total charge of *ca*. 0.1 C (Fig. 4 (e)), we can estimate that a total of 10^{18} electrons have been consumed in the film growth. The number of "sheets" is therefore $10^{18}/10^{16}$ and given that each sheet is separated ca. 10 Å, we can estimate that we should produce a 100 nm thick film. However, because some of the material crashes out in solution and the films also contain V(III) ions, this is difficult to estimate – not even taking into account the morphology of the films.

3.3 Spectroelectrochemistry

The spectroelectrochemical data are presented in Fig. 5 and the voltages should be referenced to the CV in Fig. 2 (b). At the onset of the first reduction wave at *ca*. −0.5 V in the CV in Fig. 2 (b), there is a decrease in the transmittance at 540 nm (Fig. 5 (a)). This decrease corresponds to an increase in the absorption associated with the Cr(III) to V(II) MMCT. This decrease in the transmittance grows up to −0.85 V, in agreement with the wave shown in the CV in Fig. 2 (b). This is the reason for assigning the first reduction wave in Section 3.1 to reducing V(III) to V(II). When changing the potential further to the second reduction peak at −1.22 V, the peak in transmittance at 465 nm, which gives rise to the blue colour of the V-Cr PBA, is significantly reduced in intensity (Fig. 5 (b)). As previously discussed, this is attributed to the reduction of the Cr sites. When assigning the transition associated with the loss of transmittance at 465 nm, one has to consider that the total energy of the Cr sites will increase when an extra electron is added in the reduction process. An increase in energy of the Cr ions will cause a red-shift of the MMCT transitions that occur at 540 and 660 nm. It is therefore not plausible that the new absorption feature is due to a shifted MMCT transition. The slight increase in transmittance at these wavelengths (540 – 660 nm) do support this red-shift because a loss of chromophores absorbing in the visible region would contribute to the increase in transmittance in this spectral region. The shifted MMCT is probably pushed to wavelengths longer than 900 nm, where our detection system and light source are not effective. Likewise, the LMCT states around 400 nm [21,22] would be shifted to even shorter wavelengths if the energy of the Cr ion increased. What is more, we

also rule out metal-centred transitions based on the strong absorption coefficient associated with the new absorption feature (comparable to the MMCT transitions). The increase in energy of the Cr ion upon reduction will bring it closer in energy to the empty π* orbitals on the cyanide ligands. We therefore assign the new absorption at 465 nm to MLCT transition from $[Cr^{II}(CN)_6]$ to empty π* ligand states. The peak at 800 nm has previously been assigned to a forbidden metal-centred absorption on the $[Cr^{III}(CN)_6]$ unit[19]. When Cr(III) sites are reduced, there is an increase in transmission at 800 nm, which is consistent with a loss of absorption from this transition.

3.4 Electrochromic switching

The change in colour was noticeable while carrying out the CV scans in the voltage range where $[Cr^{III}(CN)_6]$ is reduced (Fig. 6 (a) and (b)). The colour could be cycled between blue and black repeatedly and we therefore characterised the electrochromic properties of the films. The potential was cycled between 0 and −1.3 V and the charge density was recorded (Fig. 6 (c)). The transmittance at 465 nm was also recorded simultaneously. For the chosen film, the transmittance at 465 nm was T = 25 % while blue and could be reduced to ca. 3 % while black (Fig. 6 (d)). The colouration efficiency $\eta = \Delta \mathrm{OD}/\Delta \mathrm{Q}$ is typically used to characterise the efficiency of the switching process and relates to the change in optical density (ΔOD) per unit charge density ΔQ passed through the material. We follow the convention of defining η for absorbance (and therefore OD) instead of transmittance. The OD as a function of supplied charge density to the films can be plotted and the slope gives η, which is shown in Fig. 7 (a). A linear relationship of the optical density vs. charge density was found for the blue to black switching. This is because the films did not

turn completely black within the time of the switching (cf. the spectroelectrochemical data in Fig. 5 (b) where the transmittance approaches T ≈ 0.2 %). From the slope we found that $\eta = -25.2 \pm 0.2$ cm^2 C^{-1}. The switching process was rather slow and to switch from blue to black, corresponding to when the transmittance had reached 90 % of its final value, took 6.6 s. In order to keep charge-neutrality in the reduced films, electrolyte counter ions have to diffuse into the lattice. On the other hand, the switching time is almost 1.5 times faster (4.7 s) when switching from black to blue colour. For switching from black to blue, the optical density saturates with applied charge density as is seen in Fig. 7 (b). The linear part of the curve was therefore fitted to obtain $\eta = -32 \pm 1$ cm^2 C^{-1}.

4 Conclusions

In conclusion, we have synthesised thin films of the V-Cr PBA using electrochemistry and studied their optical properties using spectroelectrochemistry. We have shown that we can reduce V(III) to V(II) and observe its effect on the optical spectrum due to the spectral sensitivity of the MMCT on V oxidation state. This can be useful for electrically fine-tuning the blue colour of V-Cr PBA films and its magnetic properties. By applying a more negative voltage, we can reduce the Cr ions and control the energy of the MLCT transition, shifting it from the UV to the visible region of the spectrum. This causes the film to turn black and the colour can be cycled repeatedly. In the electrosynthesis we can control the optical density of the films by increasing or decreasing the film thickness by adjusting the deposition time. We have found that potentiostatic deposition at large negative potential leads to optically clear films with no K^+ counter ions and few vacant sites. We have demonstrated that we can

electrically control and tune the colour of a room-temperature molecule-based magnet. Combining electrical, optical, and magnetic functionality of smart materials can potentially lead to new technologies such as magneto-optical data storage devices.

Acknowledgements

The authors thank M. Verdaguer and C. Desplanches for helpful advice regarding the synthesis and characterisation of the materials, and D. Matselyukh for help with some of the measurements. This work was supported by funding from the Royal Society of Edinburgh and EPSRC (studentship to LH). JOJ is a Royal Society of Edinburgh/BP Trust research fellow.

References

[1] P.R. Somani, S. Radhakrishnan, Electrochromic materials and devices: present and future, Mater. Chem. Phys. 77 (2003) 117–133. doi:10.1016/S0254-0584(01)00575-2.

[2] R.J. Mortimer, Electrochromic Materials, Annu. Rev. Mater. Res. 41 (2011) 241–268. doi:10.1146/annurev-matsci-062910-100344.

[3] T. Nuida, T. Hozumi, W. Kosaka, S. Sakurai, S. Ikeda, T. Matsuda, H. Tokoro, K. Hashimoto, S. Ohkoshi, Colored magnetic films composed of cyano-bridged metal assemblies and magneto-optical functionalities, Polyhedron. 24 (2005) 2901–2905. doi:10.1016/j.poly.2005.08.023.

[4] A. Llordés, Y. Wang, A. Fernandez-Martinez, P. Xiao, T. Lee, A. Poulain, O. Zandi, C.A. Saez Cabezas, G. Henkelman, D.J. Milliron, Linear topology in amorphous metal oxide electrochromic networks obtained via low-temperature

solution processing, Nat. Mater. 15 (2016) 1267–1273. doi:10.1038/nmat4734.

[5] M. Verdaguer, G.S. Girolami, Magnetic Prussian Blue Analogs, in: J.S. Miller, M. Drillon (Eds.), Magn. Mol. to Mater., Wiley-VCH Verlag GmbH & Co. KGaA, Weinheim, Germany, 2005: pp. 283–346. doi:10.1002/9783527620548.ch9d.

[6] K. Itaya, T. Ataka, S. Toshima, Spectroelectrochemistry and electrochemical preparation method of Prussian blue modified electrodes, J. Am. Chem. Soc. 104 (1982) 4767–4772. doi:10.1021/ja00382a006.

[7] M. Mizuno, S. Ohkoshi, K. Hashimoto, Electrochemical Synthesis of High-Tc, Colored, Magnetic Thin Films Composed of Vanadium (II/III)–Chromium (II) Hexacyanochromate (III), Adv. Mater. 8904 (2000) 1955–1958. doi:10.1002/1521.

[8] S. Ohkoshi, M. Mizuno, G. Hung, K. Hashimoto, Magnetooptical Effects of Room Temperature Molecular-Based Magnetic Films Composed of Vanadium Hexacyanochromates, J. Phys. Chem. B. 104 (2000) 9365–9367. doi:10.1021/jp002002b.

[9] W.E. Buschmann, S.C. Paulson, C.M. Wynn, M.A. Girtu, A.J. Epstein, H.S. White, J.S. Miller, Reversed (Negative) Magnetization for Electrochemically Deposited High- T c Thin Films of Chromium Hexacyanide Magnets, Chem. Mater. 10 (1998) 1386–1395. doi:10.1021/cm970773v.

[10] E. Coronado, M. Makarewicz, J.P. Prieto-Ruiz, H. Prima-García, F.M. Romero, Magneto-optical properties of electrodeposited thin films of the molecule-based magnet Cr(5.5) (CN)(12) ·11.5H(2) O., Adv. Mater. 23 (2011) 4323–6. doi:10.1002/adma.201101513.

[11] J.P. Prieto-Ruiz, F.M. Romero, H. Prima-García, E. Coronado, Exchange coupling in an electrodeposited magnetic bilayer of Prussian blue analogues, J. Mater. Chem. C. 3 (2015) 11122–11128. doi:10.1039/C5TC01926E.

[12] P.M.S. Monk, R.J. Mortimer, D.R. Rosseinsky, Electrochromism by intervalence charge-transfer coloration: metal hexacyanometallates, in: Electrochromism and Electrochromic Devices, Cambridge University Press, Cambridge, 2007: pp. 282–302.

[13] O. Sato, T. Iyoda, A. Fujishima, K. Hashimoto, Electrochemically Tunable Magnetic Phase Transition in a High-Tc Chromium Cyanide Thin Film, Science (80-.). 271 (1996) 49–51. doi:10.1126/science.271.5245.49.

[14] O. Sato, Electrochromism and electrochemical magnetism in Ni–Fe Prussian blue, J. Solid State Electrochem. 11 (2007) 773–779. doi:10.1007/s10008-006-0203-2.

[15] Y. Mizuno, M. Okubo, K. Kagesawa, D. Asakura, T. Kudo, H. Zhou, K. Oh-ishi, A. Okazawa, N. Kojima, Precise Electrochemical Control of Ferromagnetism in a Cyanide-Bridged Bimetallic Coordination Polymer, Inorg. Chem. 51 (2012) 10311–10316. doi:10.1021/ic301361h.

[16] S. Ferlay, T. Mallah, R. Ouahès, P. Veillet, M. Verdaguer, A room-temperature organometallic magnet based on Prussian blue, Nature. 378 (1995) 701–703. doi:10.1038/378701a0.

[17] M. Verdaguer, M. Glavez, R. Garde, C. Desplanches, Electrons at Prussian Blue Work in Analogues, Electrochem. Soc. Interface. 11 (2002) 28.

[18] M. Verdaguer, A. Bleuzen, C. Train, R. Garde, F. Fabrizi de Biani, C.

Desplanches, Room-temperature molecule-based magnets, Philos. Trans. R. Soc. A Math. Phys. Eng. Sci. 357 (1999) 2959–2976. doi:10.1098/rsta.1999.0476.

[19] R. Garde, F. Villain, M. Verdaguer, Molecule-based room-temperature magnets: catalytic role of V(III) in the synthesis of vanadium-chromium Prussian blue analogues., J. Am. Chem. Soc. 124 (2002) 10531–10538. http://www.ncbi.nlm.nih.gov/pubmed/12197755.

[20] Ø. Hatlevik, W.E. Buschmann, J. Zhang, J.L. Manson, J.S. Miller, Enhancement of the Magnetic Ordering Temperature and Air Stability of a Mixed Valent Vanadium Hexacyanochromate(III) Magnet to 99 °C (372 K), Adv. Mater. 11 (1999) 914–918. doi:10.1002/(SICI)1521-4095(199908)11:11<914::AID-ADMA914>3.0.CO;2-T.

[21] K.D. Bozdag, J.-W. Yoo, N.P. Raju, A.C. McConnell, J.S. Miller, A.J. Epstein, Optical control of magnetization in a room-temperature magnet: V-Cr Prussian blue analog, Phys. Rev. B. 82 (2010) 94449. doi:10.1103/PhysRevB.82.094449.

[22] J.O. Johansson, J.-W. Kim, E. Allwright, D.M. Rogers, N. Robertson, J.-Y. Bigot, Directly probing spin dynamics in a molecular magnet with femtosecond time-resolution, Chem. Sci. 7 (2016) 7061–7067. doi:10.1039/C6SC01105E.

[23] S. Ohkoshi, Y. Einaga, A. Fujishima, K. Hashimoto, Magnetic properties and optical control of electrochemically prepared iron-chromium polycyanides, J. Electroanal. Chem. 473 (1999) 245–249. doi:10.1016/S0022-0728(99)00173-4.

[24] S. Ferlay, T. Mallah, R. Ouahes, P. Veillet, M. Verdaguer, A Chromium-

Vanadyl Ferrimagnetic Molecule-Based Magnet: Structure, Magnetism, and Orbital Interpretation, Inorg. Chem. 38 (1999) 229–234. doi:10.1021/ic980109w.

Figures

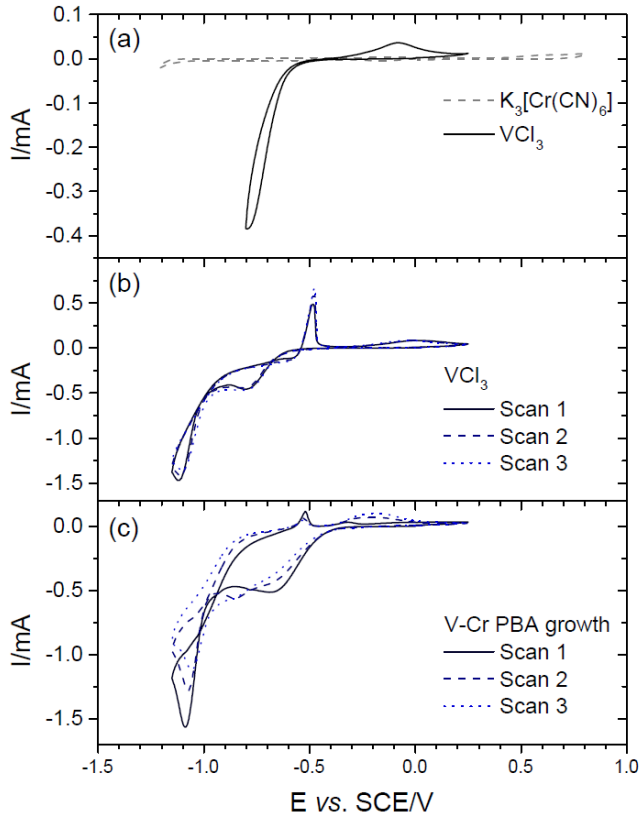

Fig.1: Cyclic voltammograms of the starting materials and the final V-Cr PBA film. (a) CV of individual starting materials. Note that the voltage range for VCl_3 is smaller than $K_3[Cr^{III}(CN)_6]$ due to additional processes taking place at more negative potentials, which is presented in (b). The CV-growth of V-Cr PBA in the presence of both starting materials is presented in (c).

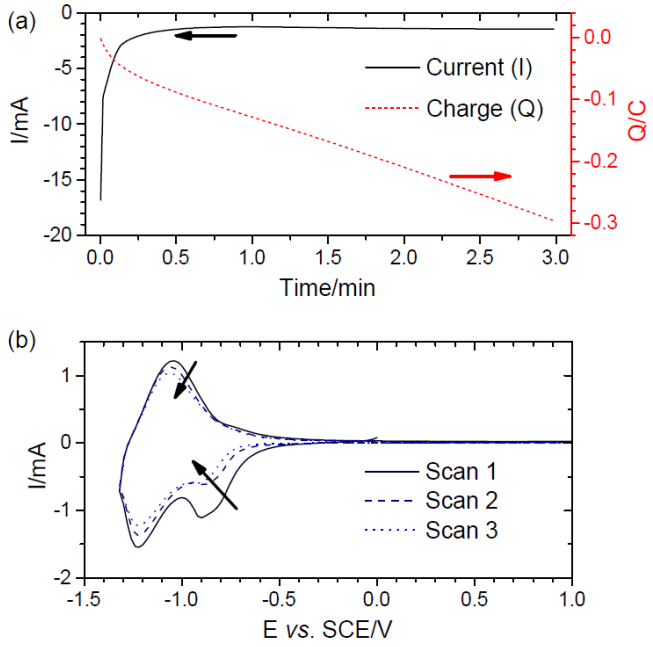

Fig.2: Charge, current, and CV of potentiostatically synthesised films. (a) The charge and current recorded during the synthesis of a V-Cr PBA film at −1.15 V for 3 minutes. The CV of the film in (a) is presented in (b).

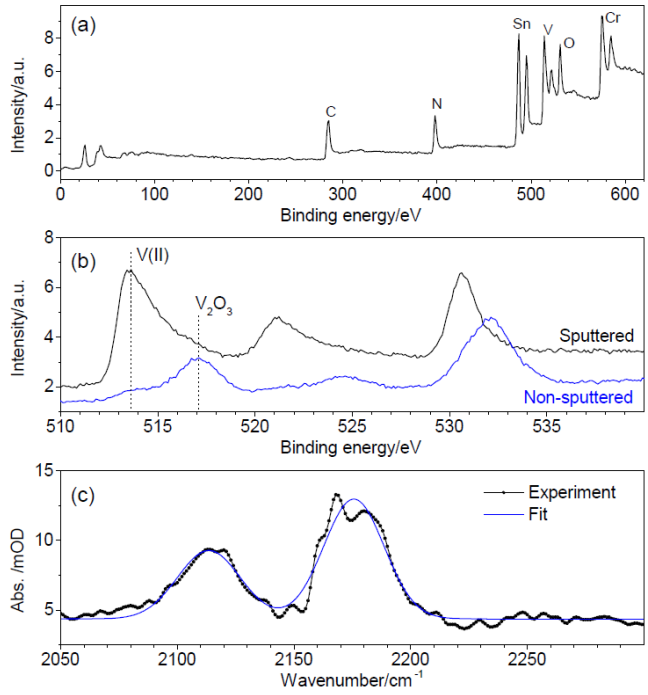

Fig. 3: XPS and IR characterisation of the V-Cr PBA films. (a) Full XPS scan of the sputtered surface, where peaks assignments are shown in the figure. The peaks to

higher binding energies for Sn, V, and Cr are due to the spin-orbit splitting. XPS spectra were also collected with a higher resolution and the region of the V $2p_{3/2}$ and $2p_{1/2}$ are shown in (b). In this region the peak for O 1s is also observed. The O 1s binding energy for the sputtered sample is closer to what is typically observed for metal oxides whereas for the non-sputtered surface it is closer to what is typically found in organic molecules (resulting from impurities on the surface). Spectra for both the un-treated and sputtered surface are shown. The IR spectrum of a V-Cr PBA film is shown in (c). The peak at 2113.5 cm^{-1} is due to the cyanide stretching mode in the $V^{II/III}$-Cr^{III} PBA. During the measurement the sample was exposed to air and became partially oxidised, which is seen as a shift of the cyanide stretching peak to 2175 cm^{-1}.

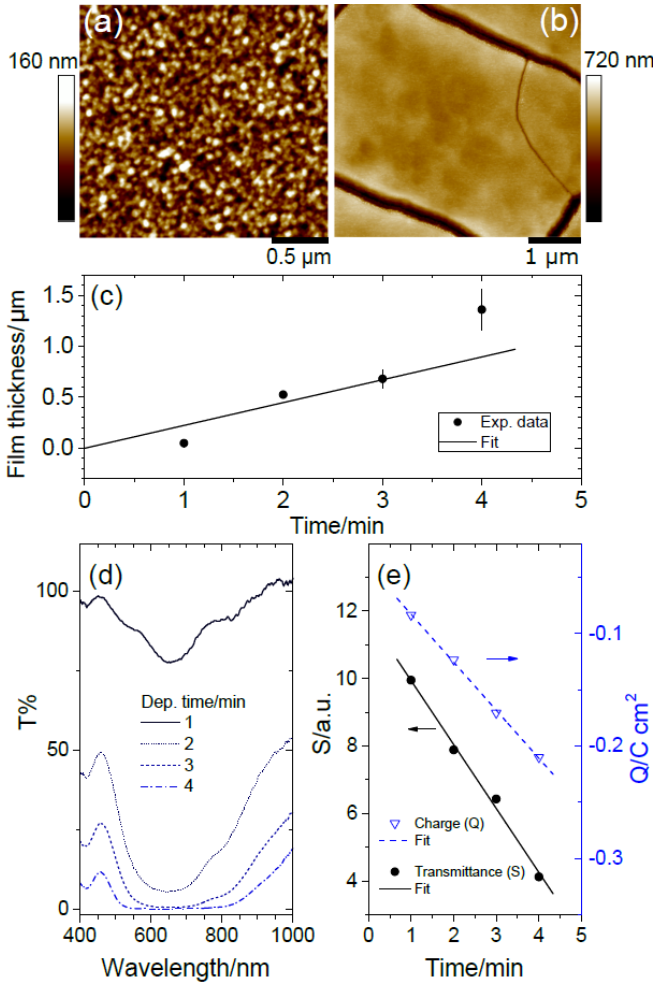

Fig. 4: Characterisation of film morphology and thickness as a function of electrochemical deposition time. All AFM measurements were carried out on oxidised samples. AFM images of films deposited for (a) 1 min and (b) 2 min are presented. The films cracked upon oxidation and the size of the crack was used to estimate the film thickness, which is plotted in (c) as a function of deposition time. Before the samples were oxidised, the optical transmittance spectra were recorded and are presented in (d). The dependence of the transmittance intensity on the film thickness is shown in (e). S is the natural logarithm of the total transmittance from 500 to 750 nm and is defined in Eq. (1). The total charge density Q used in the electrochemical synthesis is also presented in (e).

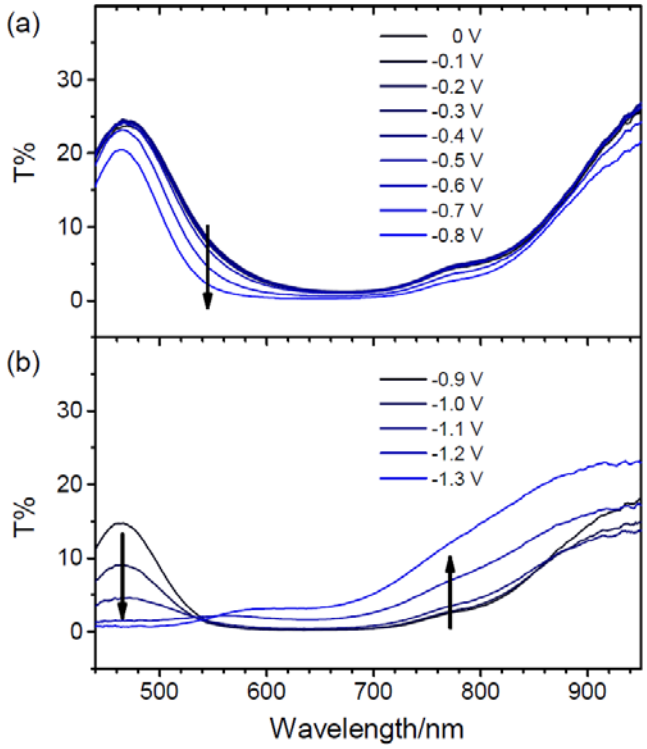

Fig. 5: Spectroelectrochemical measurements of the V-Cr PBA. For clarity the measurement is presented for two voltage regions, namely from 0 to −0.8 V (a) and from −0.9 to −1.3 V (b). Arrows indicate the direction of change in the spectra with increasing negative applied potential.

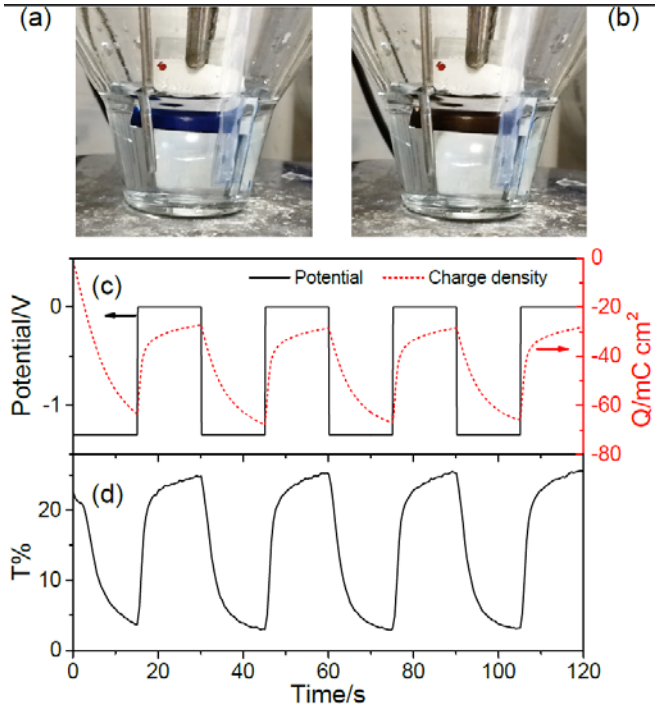

Fig. 6: Electrochromic switching of the V-Cr PBA from blue to black. Photographs of the films in the electrochemical cell (in aqueous solution of KCl) are shown in (a) at 0 V and in (b) for −1.3 V. The applied potential and corresponding charge density is presented in (c). The transmittance at 465 nm is shown in (d).

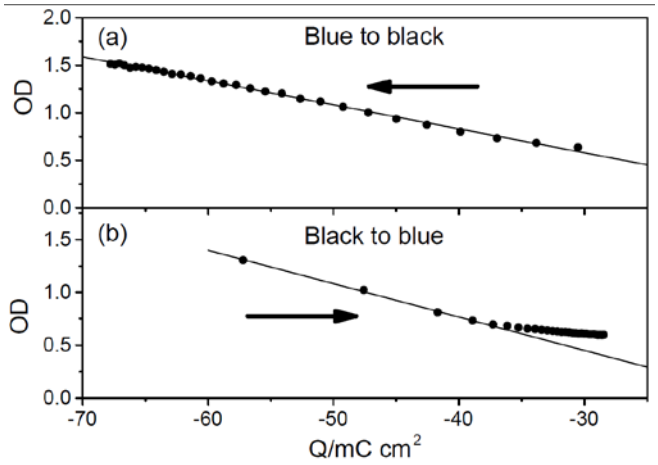

Fig. 7: The change in optical density as a function of applied charge density to the film in Fig. 5. The corresponding change from blue to black is shown in (a) and the change from black to blue is shown in (b). The chronological order of the applied charge density is indicated by the direction of the arrows.

Supplementary data

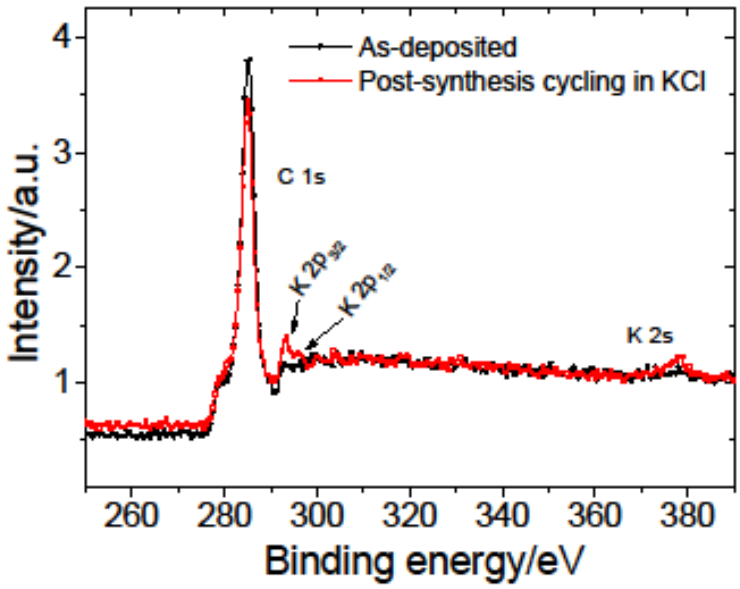

Fig. S1: XPS measurements of two V-Cr PBA films. Both films were made potentiostatically at −1.2 V for 300 s. After the synthesis, both films were rinsed with H_2O. One of the films was subsequently cycled five times in 1 M KCl solution from 0 to −1.2 V at a scan rate of 0.05 V/s. No potassium was detected in the XPS spectrum for the as-deposited film. However, a small amount potassium was observed for the cycled film. The amount was <10 % compared to the V signal although due to experimental uncertainty it was not possible to determine the absolute composition reliably. The potassium peak in the XPS spectrum of the cycled film does indicate that the charge balance during electrochemical oxidation/reduction is maintained by insertion and extraction of potassium counter ions.